A Cortico-Spinal Model of Reaching and Proprioception under Multiple Task Constraints

Paul Cisek
Boston University and Université de Montréal

Stephen Grossberg and Daniel Bullock
Boston University

Abstract

■ A model of cortico-spinal trajectory generation for voluntary reaching movements is developed to functionally interpret a broad range of behavioral, physiological, and anatomical data. The model simulates how arm movements achieve their remarkable efficiency and accuracy in response to widely varying positional, speed, and force constraints. A key issue in arm movement control is how the brain copes with such a wide range of movement contexts. The model suggests how the brain may set automatic and volitional gating mechanisms to vary the balance of static and dynamic feedback information to guide the movement command and to compensate for external forces. For example, with increasing movement speed, the system shifts from a feedback position controller to a feedforward trajectory generator with superimposed dynamics compensation. Simulations of the model illustrate how it reproduces the effects of elastic loads on fast movements, endpoint errors in Coriolis fields, and several effects of muscle tendon vibration, including tonic and antagonist vibration reflexes, position and movement illusions, effects of obstructing the tonic vibration reflex, and reaching undershoots caused by antagonist vibration. ■

INTRODUCTION

Empirical research on the control of primate reaching movements has ranged from studies of muscle activity through recordings from cells in the cerebral cortex of monkeys performing reaching tasks to observations of human movements in unusual force environments. As part of an attempt to unify these diverse experimental data, Bullock, Cisek, and Grossberg (1998) proposed a computational model that incorporates model neurons corresponding to identified cortical cell types in a circuit that reflects known anatomical connectivity (Figure 1). The model maintains accurate proprioception while controlling voluntary reaches to spatial targets, exertion of force against obstacles, posture despite perturbations, compliance with an imposed movement, and static and inertial load compensations. Computer simulations in Bullock et al. (1998) showed that properties of model elements correspond to the dynamic properties of many known cell types in areas 4 and 5 of the cerebral cortex. Among these properties are delay period activation, response profiles during movement, kinematic and kinetic sensitivities, and latency of activity onset (Alexander & Crutcher, 1990; Burbaud, Doegle, Gross, & Bioulac, 1991; Chapman, Spidalieri, & Lamarre, 1984; Cheney & Fetz, 1980; Crammond & Kalaska, 1989; Crutcher & Alexander, 1990; Evarts, 1968; Evarts, 1974; Fromm, Wise, & Evarts, 1984; Georgopoulos, Caminiti, & Kalaska, 1984; Georgopoulos, Caminiti, Kalaska, & Massey, 1983; Georgopoulos, Kalaska, Caminiti, & Massey, 1982; Kalaska, Cohen, Hyde, & Prud'homme, 1989; Kalaska, Cohen, Prud'homme, & Hyde, 1990; Kalaska & Crammond, 1992; Kalaska & Hyde, 1985; Kettner, Schwartz, & Georgopoulos, 1988; Lacquaniti, Guigon, Bianchi, Ferraina, & Caminiti, 1995; Schwartz, 1992; Schwartz, 1993; Scott & Kalaska, 1997). The model also reproduces various psychophysical phenomena, such as bell-shaped velocity profiles, speed-accuracy trade-offs, and characteristics of deafferented operation (Atkeson & Hollerbach, 1985; Bizzi, Accornero, Chapple, & Hogan, 1984; Fitts, 1954; Woodworth, 1899).

This report describes how the model (Figure 1) can be applied to explain additional phenomena, including several that have seemed anomalous from a functional perspective. These include proprioceptive illusions and numerous other effects of muscle tendon vibration, including the tonic and antagonist vibration reflexes (TVR and AVR) and reaching inaccuracies; properties of fast movements with elastic loads; and endpoint errors in Coriolis fields (Capaday & Cooke, 1981; Capaday &

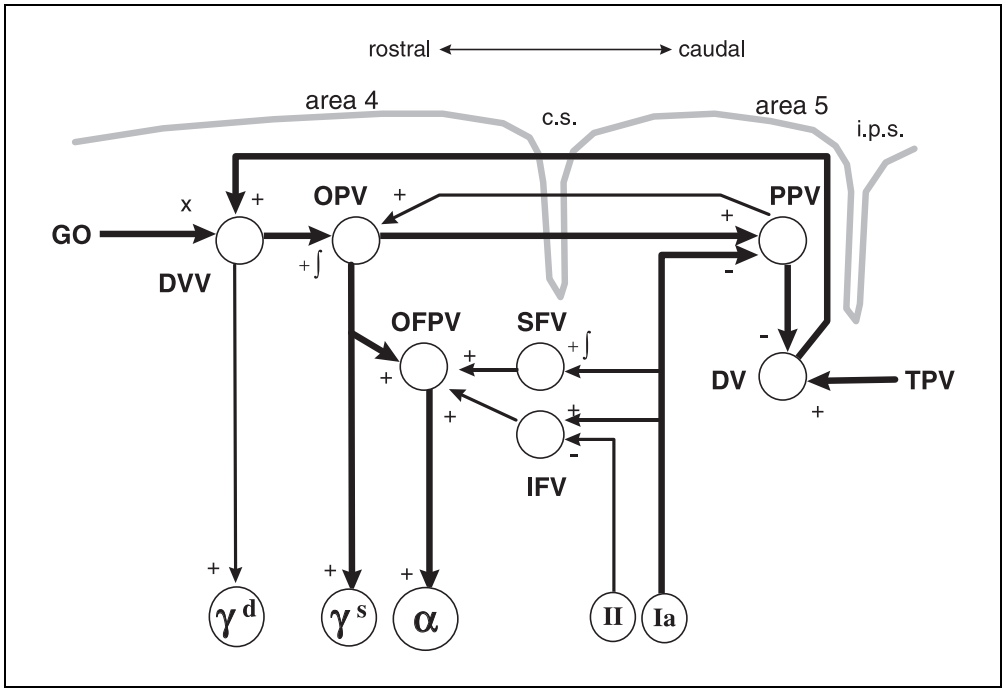

Figure 1. Circuit diagram of the model. Thick connections represent the kinematic feedback control aspect of the model, with thin connections representing additional compensatory circuitry. GO—scalable gating signal; DVV—desired velocity vector; OPV—outflow position vector; OFPV—outflow force + position vector; SFV—static force vector; IFV—inertial force vector; PPV—perceived position vector; DV—difference vector; TPV—target position vector; γ^d—dynamic gamma motor neuron; γ^s—static gamma motor neuron; α—alpha motor neuron; Ia—type-Ia afferent fiber; II—type-II afferent fiber; c.s.—central sulcus; i.p.s.—intraparietal sulcus. The symbol + represents excitation, − represents inhibition, × represents multiplicative gating, and +∫ represents integration.

Cooke, 1983; Feldman, Adamovich, & Levin, 1995; Gilhodes, Roll, & Tardy-Gervet, 1986; Goodwin, McCloskey, & Matthews, 1972b; Hagbarth & Eklund, 1966; Lackner & DiZio, 1994).

The extensions to the model introduced in this report add no new cell types, or any new connections, to that introduced in Bullock et al. (1998). Instead, they suggest how the brain adjusts the gains on otherwise fixed movement pathways to optimize the balance of cooperating mechanisms in different operating contexts. This hypothesis is in keeping with evidence that neural circuits for sensory-motor control can often operate in a number of distinct modes (Humphrey & Reed, 1983; Loeb, 1985; Prochazka, 1992; Saltzman & Kelso, 1987; Selverston, 1988), which are sometimes discussed in terms of how the brain controls sensory-motor set (e.g., Evarts, 1974). Thus, a single circuit for trajectory generation and posture maintenance can exhibit various operating modes as determined by other centers that influence pathway gains.

The following hypotheses summarize the model (Bullock, Cisek, & Grossberg, 1998):

1. An arm movement difference vector (DV) is computed in parietal area 5 from a comparison of a target position vector (TPV) with a vector representation of perceived arm position (PPV). The DV command may be activated, or primed, prior to its overt performance.

2. The PPV is also computed in area 5, where it is derived by subtracting spindle-based feedback of position error, which is routed to area 5 via area 2, from an efference copy of an outflow position vector (OPV) from area 4.

3. The primed DV projects to a desired velocity vector (DVV) in area 4. A voluntarily scalable GO signal gates the DV input to the DVV in area 4. By virtue of the scaled gating signal, the phasic cell activity of the DVV serves as a volition-sensitive velocity command, which activates lower centers including gamma-dynamic motor neurons.

4. The DVV command is integrated by a tonic cell population in area 4, whose activity serves as an outflow position vector (OPV) to lower centers, including alpha and static gamma motor neurons. This area 4 tonic cell pool serves as source of the efference copy signal used in area 5 to compute the perceived position vector (PPV). As the movement evolves, the difference vector (DV) activity in area 5 is driven toward baseline. This leads to termination of excitatory input to area 4 phasic cells and thus to termination of the movement itself.

5. A reciprocal connection from the area 5 perceived position vector (PPV) cells to the motor-cortical tonic cells (OPV) enables the area 4 position command to track any movement imposed by external forces. This reciprocal connection also helps to keep spindles loaded and to avoid instabilities that would otherwise be associated with lags due to finite signal conduction rates and loads.

6. Phasic-tonic force-related (OFPV) cells in area 4 enable graded force recruitment to compensate for static and inertial loads, using inputs to area 4 from the cerebellum and a center that integrates spindle feedback. These area 4 phasic-tonic cells enable force of a desired amount to be exerted against an obstacle without interfering with accurate proprioception (PPV) and while preserving a target position (TPV) should the obstacle give way.

Extensive evidence for the above six hypotheses was reviewed in Bullock et al. (1998). The mode switches that are needed to treat the additional experimental observations simulated below can be summarized with two additional hypotheses:

7. During fast movements, the system shifts toward a more feedforward and dynamically sensitive operating mode. This is accomplished by reducing the gain of the outflow position command (OPV) projection to static gamma motor neurons. This reduces spindle sensitivity to static position error. The same operating mode is used when quick responses to unpredictable perturbations are desired.
8. To generate the large forces needed to lift large masses (e.g., to lift the body to upright stance), the gain of the load-compensation mechanism is significantly increased during the lifting phase.

The Model Development section reviews the model and specifies its behavior through a system of differential equations. It then focuses on pathway gating operations that extend its operating modes. The Simulations section presents simulations that illustrate how these operating modes help to explain several additional sets of psychophysical observations.

MODEL DEVELOPMENT

The model of Bullock et al. (1998) elaborated the Vector-Integration-To-Endpoint (VITE) model of Bullock and Grossberg (1988). That model addressed psychophysical properties of normal human movements such as straight trajectories in 3-D space, bell-shaped velocity profiles, speed-accuracy trade-offs, and synchronization of synergists. It also discussed movement-related activities in the primary motor cortex such as directional-tuning and responses to perturbation. The Bullock et al. (1998) extension of VITE achieved broader functionality and a more detailed analysis of neural responses in cortical areas 4 and 5, as discussed below.

Cortical Circuit Model for Trajectory Generation

Figure 1 depicts the model, which uses lumped representations of neural variables postulated to be coded by activity levels distributed across cortical populations (Kalaska & Crammond, 1992). Once functional roles are clarified by a lumped analysis, the model elements can be unlumped as needed to study properties associated with distributed representations. To simplify the mathematical specification and computer simulation, only single-joint movements are treated. The model, however, is compatible with related theories of movement control that address multijoint coordination and the learning and execution of spatial-motor transformations (Bullock, Grossberg, & Guenther, 1993; Kettner, Marcario, & Port, 1993; Kuperstein, 1988), as noted in the "Discussion."

Limb dynamics are described by the following equation:

$$\frac{d^2p_i}{dt^2} = \frac{1}{I}\left(M(c_i\,,p_i) - M(c_j\,,p_j) + E_i - V\frac{dp_i}{dt}\right) \qquad (1)$$

where p_i is the position of a muscle i within its range of origin-to-insertion distances, and $p_j = 1 - p_i$ is the position of the antagonist muscle j within its range. Indices i and j are used in this way throughout. For simplicity, the position ranges from 0 to 1, with 1 the maximally compressed state of the muscle and 0 its maximally extended state. The parameter V is the joint viscosity and I is the limb moment of inertia. External forces are represented by E_i, which is positive if the force assists movement in the ith direction and negative if it opposes.

The muscle function $M(\cdot)$ gives the force generated by a muscle given some contractile activity c_i and the position p_i. For simplicity, geometric effects due to moment arm, muscle yielding, and nonlinearities of force generation are ignored (see Bullock & Grossberg, 1991 for one treatment of these factors). The *muscle force* equation

$$M(c_i,p_i) = [L_i + M_i - \Gamma_i]^+ \qquad (2)$$

depends on the length L_i of the muscle, the contraction level M_i, and the muscle resting length Γ_i. The threshold-linear function $[w]^+$ is defined as $\max(w,0)$. Defining $L_i = 1 - p_i$ and $\Gamma_i - M_i = 1 - c_i$ yields the muscle force function

$$M(c_i,p_i) = [c_i - p_i]^+ \qquad (3)$$

The *contractile* activity c_i is governed by

$$\frac{dc_i}{dt} = \upsilon(-c_i + \alpha_i) \qquad (4)$$

where α_i represents alpha motor neuron activity, and υ scales the contraction rate.

The remainder of the system affects the limb by adjusting the alpha motor neuron activities. For voluntary movements, the system operates via area 4. The process of assembling the net descending command to alpha motor neurons can be divided conceptually into kinematic and kinetic aspects, of which the former is treated first. The kinematic aspect of trajectory control involves specifying the time series of positions that the limb is intended to occupy between its initial and its desired final position. Guided by neurophysiological data (Fromm, Wise, & Evarts, 1984; Kalaska, Cohen, Hyde, & Prud'homme, 1989; Kettner, Schwartz, & Georgopoulos, 1988), Bullock et al. (1998) proposed that tonic cells in area 4 correspond to this intended position command, and model their activity by

$$\frac{dy_i}{dt} = (1 - y_i)(\eta x_i + [u_i - u_j]^+) - y_i(\eta x_j + [u_j - u_i]^+) \quad (5)$$

where y_i is the average firing rate of a population of area 4 tonic cells called the *Outflow Position Vector* (OPV), ui is the activity of area 4 phasic movement-time (MT) cells called the Desired Velocity Vector (DVV), x_i is the activity of anterior area 5 cells called the Perceived Position Vector (PPV), and η is the gain on a pathway from the PPV to the OPV. The DVV and PPV cell populations are described below. Without input from the PPV, Equation 5 says that the tonic cell population (OPV) integrates the DVV inputs. Activation increments and decrements depend on the difference between the agonist (u_i) and antagonist (u_j) phasic-MT activities. Activity ranges between 0 and 1, and $y_i + y_j = 1$. Without input from the DVV, Equation 5 says that the tonic cell population (OPV) tracks the PPV activation pattern. This pathway acts to release tension and comply with external forces when the system is in a passive state. When both inputs to the OPV are active, the Outflow Position Vector shifts in the direction specified by the DVV while responding to information about externally imposed demands specified by the PPV. The active and passive states produced by these pathways are described in more detail below.

The DVV in area 4 is interpreted to be a gated and scaled version of a movement command that is continuously computed in posterior area 5 as the vector difference between the target and the perceived limb position vectors. Area 5 *Difference Vector* (DV) cell activity can be described by

$$r_i = [T_i - x_i + B^{(r)}]^+ \quad (6)$$

where r_i is the activity of a DV cell, and $B^{(r)}$ is its baseline activity. The target position vector (TPV) is expressed as T_i and current limb position (PPV), as x_i. These model area 5 cells fire at the baseline rate except when current and targeted limb position differ, such as during movement and movement priming intervals. The proposal that posterior area 5 phasic cells carry such a Difference Vector signal is based upon their tuning to movement direction, onset timing, and primability (Burbaud, Doegle, Gross, & Bioulac, 1991; Chapman, Spidalieri, & Lamarre, 1984; Crammond & Kalaska, 1989; Kalaska, Cohen, Prud'homme, & Hyde, 1990; Lacquaniti, Guigon, Bianchi, Ferraina, & Caminiti, 1995).

Computation of perceived position depends on both central commands and feedback from muscle receptors. (Visual feedback is not treated here.) This function is proposed to be performed by tonic cells in anterior area 5, which relate to the position of the limb, are load-insensitive, and whose activity follows movement initiation (Burbaud, Doegle, Gross, & Bioulac, 1991; Kalaska, Cohen, Prud'homme, & Hyde, 1990; Kalaska & Hyde, 1985; Lacquaniti, Guigon, Bianchi, Ferraina, & Caminiti, 1995). The following equations describe the computation of a *Perceived Position Vector* (PPV) by anterior area 5 tonic cells that are assumed to receive an efference copy input from area 4 and position error feedback from muscle spindles:

$$\frac{dx_i}{dt} = (1 - x_i)\left[\Theta y_i + s_j^{(1)}(t - \tau) - s_i^{(1)}(t - \tau)\right]^+ - x_i\left[\Theta y_j + s_i^{(1)}(t - \tau) - s_j^{(1)}(t - \tau)\right]^+ \quad (7)$$

$$\gamma_i^S = \chi y_i \quad (8)$$

$$\gamma_i^D = \rho u_i \quad (9)$$

$$s_i^{(1)} = S\left(\theta[\gamma_i^S - p_i]^+ + \phi[\gamma_i^D - \frac{dp_i}{dt}]^+\right) \quad (10)$$

where x_i is the average firing rate over a population of anterior area 5 tonic cells (PPV), γ_i^S and γ_i^D are the activities of static and dynamic gamma motor neurons, χ and ρ are gain parameters, $s_i^{(1)}$ is the activity of primary spindle afferents from muscle *i*, θ is the sensitivity to a stretch of the static nuclear bag and chain fibers, ϕ is the sensitivity of dynamic nuclear bag fibers to rate of stretch, and Θ is the gain of the corollary discharges from area 4 tonic cells, calibrated such that $\Theta \approx \theta$ to ensure accurate PPV calculation. The variable t represents the time step, and parameter τ is the delay on the feedback from spindles to central sites. Because $y_j = 1 - y_i$ and $p_j = 1 - p_i$, Equation 7 implies that x_i tracks position p_i at rate Θ, while integrating velocity errors to correct the estimation of the position.

The function $S(\cdot)$ in Equation 10 expresses the limited dynamic range of spindle afferent activity and is defined by the following equation:

$$S(w) = \frac{w}{1 + 100w^2} \quad (11)$$

Equation 11 implies that feedback signals from spindles are linear near the low end of their dynamic range but begin to saturate around 0.04 (i.e., around 4% of the full joint range).

Figure 2 illustrates how muscle spindles can be used to compute a positional error. Spindles have long been recognized to respond sensitively to small but not large stretches, and it has been argued (Kuffler & Hunt, 1952) that the intrafusal contraction serves to maintain spindle sensitivity by resetting the base length relative to which the spindle can sensitively register the degree (or rate) of stretch. This is equivalent to saying that, to maintain

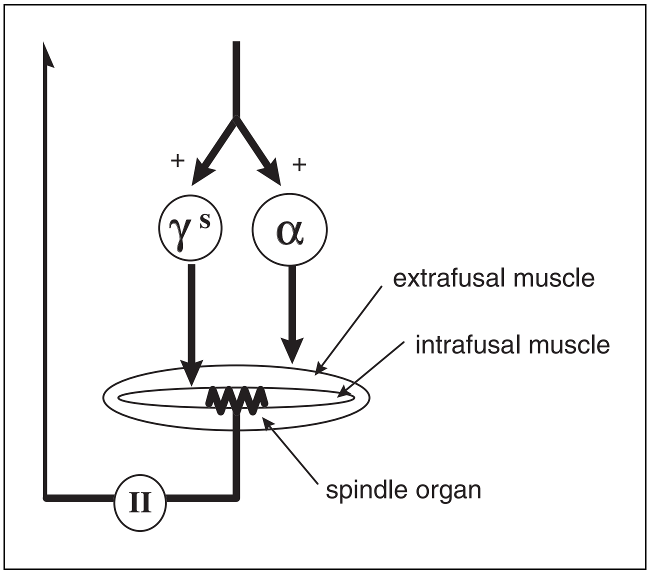

Figure 2. Spindle computation of positional error. Alpha and gamma-static motor neurons receive a desired contraction command. If the extrafusal muscle is kept from contracting, the spindle organ is stretched by the contraction of the intrafusal muscle and secondary spindle afferents report a position error.

sensitivity, the intrafusal length is set to the expected length of the extrafusal, in which case an above baseline spindle firing rate will indicate a positive length discrepancy of the extrafusal ("stretch") and a below baseline spindle discharge rate will indicate a negative length discrepancy of the extrafusal muscle ("excess contraction"). During voluntary movement, if the intrafusal length is continuously updated to reflect the desired extrafusal length, the measured length discrepancies can serve as a signed error feedback to the neural controller. If a load retards movement unexpectedly, the spindle response may saturate in the agonist and fall silent in the antagonist, but the sign of the error feedback will remain accurate.

A similar scheme is used to compute velocity errors by the spindles, with a projection of desired velocity from the DVV to dynamic gamma motor neurons, resulting in type-Ia afferents carrying both position and velocity error information, as specified by Equation 10.

The model proposes that a gating operation allows DV movement priming to be translated into an overt movement. Gating is represented mathematically by multiplying the DV activities by a scalar GO signal to yield the *Desired Velocity Vector* (DVV), as described by the following equation:

$$u_i = [g \cdot (r_i - r_j) + B^{(u)}]^+ \qquad (12)$$

where u_i is the area 4 phasic MT cell activity (DVV), r_i is the DV, g is the GO signal, and $B^{(u)}$ is the baseline activity for the DVV. Phasic movement-time (MT) cells in area 4 are a likely candidate for a DVV-like computation because their activity profiles resemble a bell-shaped velocity profile, they are tuned to direction of movement, and they show little load-sensitivity (Fromm, Wise, & Evarts, 1984; Georgopoulos, Kalaska, Caminiti, & Massey, 1982; Kalaska, Cohen, Hyde, & Prud'homme, 1989).

The GO signal is assumed not to turn on abruptly but rather to exhibit sigmoidal growth during the movement generation interval. For simplicity, equations for a two-step cellular cascade were used to generate the sigmoidal GO signal:

$$\frac{dg^{(1)}}{dt} = \varepsilon[-g^{(1)} + (C - g^{(1)})\, g^{(0)}]$$

$$\frac{dg^{(2)}}{dt} = \varepsilon[-g^{(2)} + (C - g^{(2)})\, g^{(1)}]$$

$$g = g^{(0)} \frac{g^{(2)}}{C} \qquad (13)$$

where g is the GO signal that multiplies the Difference Vector (see Equation 12, above), $g^{(0)}$ is the step input from a forebrain decision center, ε is a slow integration rate, and C is the value at which the GO cells saturate. Any cascade larger than 2 will also generate a sigmoidal GO signal. An analysis of GO signal shape and its effect on the bell-shaped velocity profile and other properties observed during movements can be found in prior reports (Bullock & Grossberg, 1988).

With system of Equations 1 through 13, inertial effects can cause the limb's trajectory to show transient mismatches with the trajectory specified by the evolving OPV. The limb can lag the OPV at the beginning of movement and overshoot the target briefly at the end. Such undesirable effects can be partly compensated by circuitry that reduces velocity errors. In the model, an *Inertial Force Vector* (IFV), identified with activity of area 4 phasic reaction-time (*RT*) cells (Kalaska, Cohen, Hyde, & Prud'homme, 1989), extracts velocity errors from the primary and secondary spindle feedback, as described by the following equation:

$$q_i = \lambda[s_i^{(1)}(t - \tau) - s_i^{(2)}(t - \tau - \Lambda)]^+ \qquad (14)$$

where λ is the feedback gain and Λ is a threshold. Secondary spindle afferents are modeled as

$$s_i^{(2)} = S(\theta[\gamma_i^s - p_i]^+) \qquad (15)$$

where $S(\cdot)$ and θ are as in Equation 10. The IFV activity q_i, is added to the Outflow Position Vector and projected to alpha motor neurons as described by Equations 17 and 18, below. This means that the velocity errors that occur as rest inertia is being overcome at the beginning of movement are translated into a launching pulse that generates extra force in the agonist extrafusal muscle, helping to get the limb moving. The same velocity errors generate a braking pulse in the antagonist that helps to slow the limb at the end of movement as momentum

causes it to move faster than the decreasing Desired Velocity Vector.

To compensate for static loads such as gravity, the model integrates positional errors reported by the spindles and adds these to the alpha motor neuron command. Spindle error integration is performed by a *Static Force Vector* (SFV), which is described by

$$\frac{df_i}{dt} = (1 - f_i)h \cdot \kappa_i \cdot s_i^{(1)}(t - \tau) - \psi f_i \left[f_j + s_j^{(2)}(t - \tau) \right] \quad (16)$$

where h is a gain that controls the strength and speed of load compensation (modulated by a muscle-specific gain κ_i), and ψ is a parameter scaling inhibition by the antagonist component of the SFV and by the antagonist spindle. At present, no cortical cellular analogue is proposed for the SFV, but the connectivity of this model component to identified cells may provide a road map for discovering it through a combination of staining and physiological techniques.

Bullock et al. (1998) proposed that area 4 phasic-tonic cells assemble a shifting positional command (OPV) with inertial (IFV) and static (SFV) load compensating commands, to yield a command to alpha motor neurons that produces the desired kinematic result under variable external forces. The activity of phasic-tonic cells constitutes an *Outflow Force + Position Vector* (OFPV) and is described by

$$a_i = y_i + q_i + f_i \quad (17)$$

An alpha-command assembly role for phasic-tonic cells in area 4 seems reasonable because they are highly load sensitive and relate both to the position and force of a movement (Fromm, Wise, & Evarts, 1984; Kalaska, Cohen, Hyde, & Prud'homme, 1989). (Although interpreted differently by the authors at the time, the data of Georgopoulos, Ashe, Smyrnis, and Taira, 1992, also show cell activities tuned to both position and force—see their Figure 2.) The most likely candidates are pyramidal tract neurons, and in particular, corticomotorneuronal cells, of which about half exhibit the phasic-tonic profile and load sensitivity expected from an OFPV command (Cheney & Fetz, 1980). After the OFPV command has been assembled, it projects to the *alpha motor neurons*

$$\alpha_i = a_i + \delta s_i^{(1)} \quad (18)$$

where δ is the gain of the stretch reflex. The OFPV command is not sent to gamma motor neurons for two related reasons. Doing so would create a positive feedback and would disrupt the error measurement function of spindles.

The system of Equations 1 through 18 can be used to generate voluntary reaching movements at variable speeds while compensating for external perturbations including inertial and static loads and transient deflections, to maintain posture against perturbations and to exert forces against objects that obstruct a reaching movement. When in a relaxed state, specified when no target representation or GO signal is given, the system passively complies with external forces while maintaining an accurate internal representation of limb position. Bullock et al. (1998) discuss how model elements exhibit properties similar to the neurophysiological properties of various cell types in cortical areas 4 and 5. This resemblance includes the activity profiles of movement-related cells, their kinematic and kinetic sensitivities, priming activity during delay periods, response to perturbations during movement, and activity onset latencies. Figure 3 illustrates simulations of these cell activities during a voluntary reaching movement.

Production of Different Operating Modes through Gating

Properties of the circuit model described above can be modified in accord with different task demands through the addition of gating mechanisms that are sensitive to task constraints. One kind of gating, volitional gating by a scalable GO signal, was explored in the simulations of Bullock and Grossberg (1988, 1991) and Bullock et al. (1998) and is briefly reprised below. Other kinds of gating are proposed below, and their effect on the behavior of the model is specified.

Gating Movement Speed and Compliance

GO signal scaling of the Difference Vector plays several roles in the system. First, it controls the onset and speed of voluntary movement by scaling the command that is integrated by the Outflow Position Vector. This can be used not only to change the average speed of the movement but also to shape the velocity profile. Use of a growing GO signal, such as that implemented by Equation 13, produces the bell-shaped velocity profile characteristic of human movements (Atkeson & Hollerbach, 1985). Second, the GO signal can be used to withhold execution of movement or to abort a movement in progress. This gives the system independent control over planning the movement target (TPV) and timing the movement execution (Bullock & Grossberg, 1988).

Third, the GO signal controls the effort with which the system resists external perturbations. This applies to several scenarios. Consider first a case where the limb is already at the target position specified by the TPV, but the GO signal remains positive. This means that any deviations from the target caused by external perturbations will result in a nonzero Difference Vector, which will immediately translate to a nonzero DVV and cause

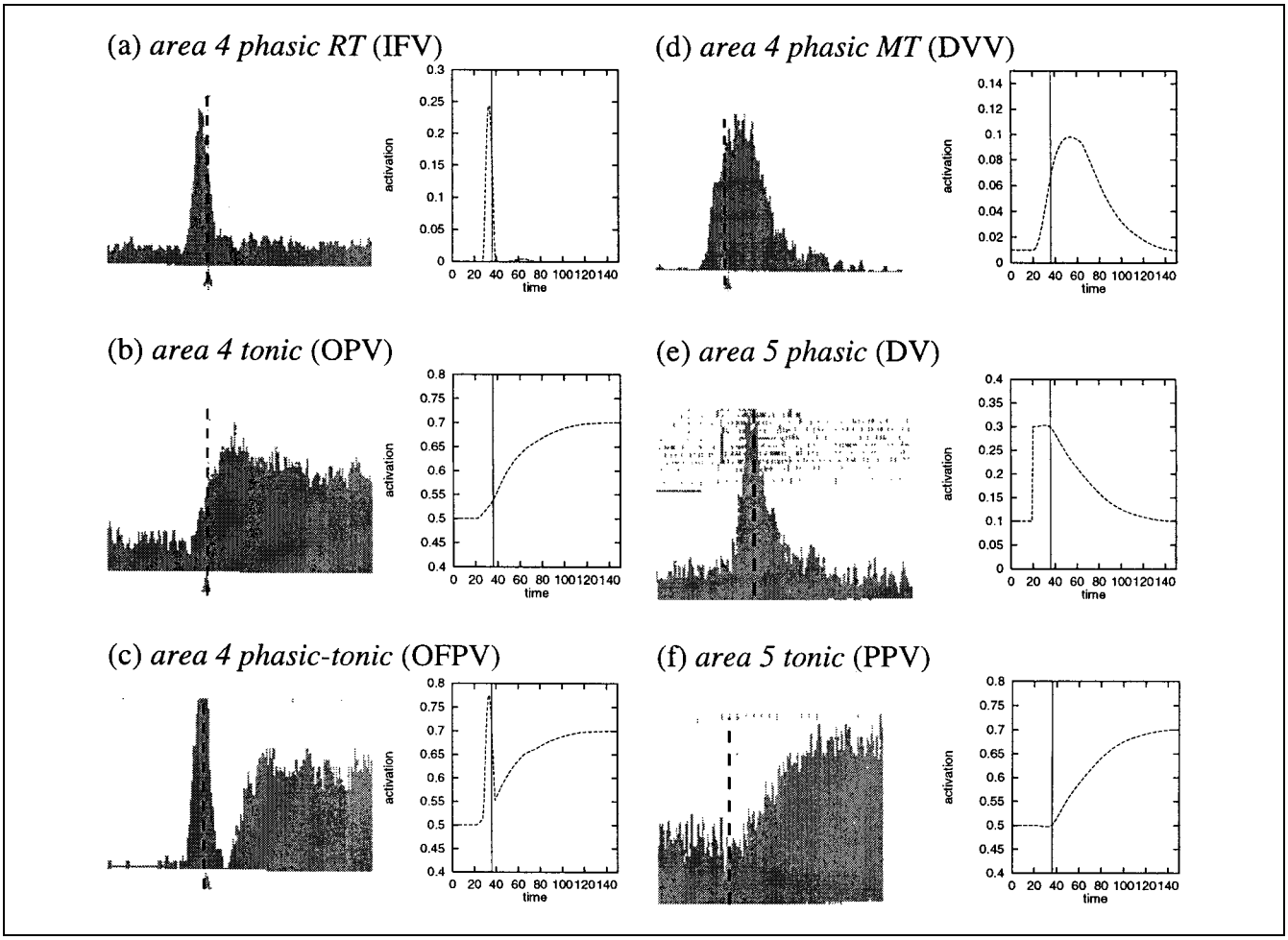

Figure 3. Comparison of cortical activity and model cell responses during a simple voluntary reaching task. Histograms in (a through d) are taken from Kalaska et al. (1989) and (e) and (f) are from Kalaska et al. (1990). Histograms are centered on the onset of movement, which is indicated in both the data and the simulations by a vertical line. In the simulations, the GO signal was set at $g^{(0)} = 0.5$. Feedforward inertial load compensation was simulated by reducing τ to 0 and increasing λ to 100. (Reprinted with permission from Bullock, Cisek, and Grossberg, 1998.)

OPV integration to bring the limb back to the target. The GO signal controls the speed of this return movement. At the same time, however, the PPV-OPV pathway will drag the OPV toward the actual deflected limb position. The final equilibrium will depend on the balance between the PPV-OPV gain and the magnitude of the GO signal. When SFV integration is enabled, load-compensation will reduce any residual errors and bring the limb to the target.

Next, consider the case where a voluntary movement is being made. Onset of the target and GO signals causes OPV integration and changes in muscle contraction patterns. If no obstacles are present, the movement proceeds as planned and the PPV reflects the changing limb position. Because the PPV is moving with the OPV, the action of the PPV-OPV pathway is minimal. This pathway helps to slow the shift of the movement command if large limb masses cause a significant lag between the PPV and the OPV, thus adjusting the trajectory generation to the external load. However, if some object obstructs further movement, the difference between the PPV and OPV will grow larger, and the PPV-OPV pathway will keep the OPV from integrating too far past the object. This helps to keep spindles from being stretched out of their sensitive range. The distance by which the OPV penetrates into the obstacle is dependent, again, on the balance between the PPV-OPV gain and the magnitude of the GO signal. Thus, the GO signal controls the effort with which the system resists obstruction.

In the absence of the GO signal, the system is in a relaxed state. This means that any movements imposed by external forces or objects cause changes in the PPV and therefore also in the OPV due to the PPV-OPV pathway, which is now its only source of input. Thus, tension on the limb is released and the system passively complies with external demands. Note that the kind of compliance control treated in this section differs from nondirectional joint compliance control, which may be

achieved by an additive cocontraction command (e.g., Bullock & Grossberg, 1991; Bullock & Contreras-Vidal, 1993).

Gating Peripheral Sensitivity

As movement speeds increase, delays in peripheral feedback become a significant concern. Position error signals arriving late are not only not helpful, but they can severely jeopardize system stability. On the other hand, velocity error signals become important for shaping launching and braking pulses. These concerns motivate the addition of a gating mechanism that controls the balance of static and dynamic information in the system's feedback pathways.

One might expect that as movement speeds increase, the motor system shifts from operating as a position controller that relies on static error signals to operating as a velocity controller dominated by a feedforward command and dynamic error feedback. Psychophysical evidence supports this view (Clark, Burgess, Chapin, & Lipscomb, 1985; Gielen & Houk, 1987; McCloskey, 1973; Sittig, Denier van der Gon, & Gielen, 1985).

Two functional rules are proposed to govern the control of the system's utilization of static and dynamic feedback signals:

1. While maintaining stationary posture, use static feedback signals to ensure accurate PPV computation.

2. When a fast voluntary movement is desired, ignore static feedback and instead use dynamic feedback (or learned feedforward compensation) to generate appropriate launching and braking pulses.

It is worthwhile to consider an additional case, where a response must be made to a perturbation, the direction of which is unpredictable. In this scenario, a quick response to the perturbation is more important than an accurate PPV representation, and the direction is of most interest. For this purpose, dynamic feedback is most useful, because it directly provides information on the direction of external perturbations. Thus, one might formulate a third rule:

3. When responding to perturbations of unpredictable direction, concentrate on dynamic feedback information.

In the model, the shift from static to dynamic feedback can be implemented in a number of ways. One is to reduce the parameter θ, which controls the sensitivity of the primary and secondary afferents to static position errors (see Equations 10 and 15), or increase the parameter ϕ, which controls primary dynamic sensitivity (see Equation 10). However, such sensitivity changes would have to occur at the spindles themselves, and it is difficult to imagine how they could be centrally controlled. Alternately, the spindle sensitivity to static information could be reduced by decreasing the parameter χ, which controls the gain of the OPV projection to static gamma motor neurons (Equation 8). Because the position error signal is computed at the spindles as a rectified difference of static gamma activity and position (see Equations 10 and 15), this signal can be reduced if the static gamma activity is reduced.

Another option is to explicitly separate the static and dynamic errors and gate their input to the PPV independently. This would allow central control of the contributions of position error feedback versus velocity error feedback to PPV computation. Such a central allocation of "attention" among signal sources is common across the nervous system and ensures that information that may be detrimental toward one function (feedback control of fast movement) is not lost to other systems to which it remains valuable (e.g., cerebellar learning sites).

Issues of bandwidth suggest that peripheral, rather than central, sensitivity should be the controlled variable. The spindle saturation function (Equation 11) implies that static and dynamic components of the primary spindle response have to compete for a limited range of firing frequency in the Ia fiber. As static signals increase, they leave less range for dynamic signals, and vice versa. Consider now the scenario described above where an organism is trying to respond to unpredictable perturbations. Its response is dominated by a decision regarding the direction of the perturbation, and this decision must be made as quickly as possible. Assuming noisy feedback, the system needs to define thresholds that the signal must cross before it is used to make the decision to respond in one direction or another (see Figure 4b).

If the static component of the spindle response is reduced, most of the Ia activity range remains available for the dynamic component. This means that a given velocity of perturbation generates a large change in the Ia feedback (see Figure 4a). In contrast, if the static component shifts the Ia response toward saturation, less activity range is available to the dynamic component. Thus, the dynamic signals are smaller and take longer to cross the threshold at which the decision to respond to the perturbation is made. Consequently, the response to perturbation is delayed.

Similar issues arise in other situations. The limited dynamic range of feedback fibers forces a trade-off between static and dynamic sensitivity that must be resolved at the level of the receptors. For this reason, it is better to control changes in utilization of static versus dynamic error signals by directly changing peripheral sensitivities rather than through a central attentional mechanism.

In the model, peripheral sensitivity is changed by varying the parameter χ, which controls the gain of the OPV projection to static gamma motor neurons (see Equation 8). When this parameter is set at 1, the spindle sensitivity to static errors is ideal for accurate computation of the PPV. As χ is reduced slightly below 1, positional errors need to exceed a small threshold before being registered by the spindle. As χ drops further, only

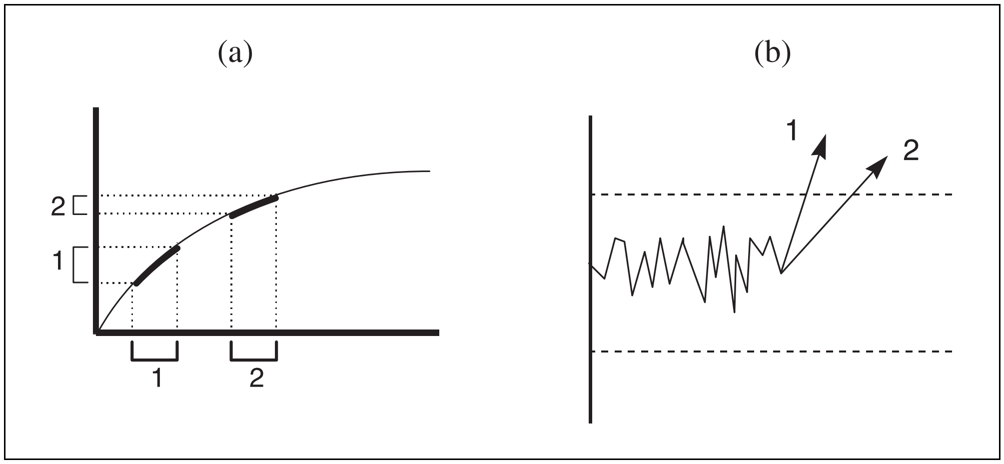

Figure 4. Trade-off between static and dynamic sensitivity. (a) Input versus output function of Ia fibers. With small static input (1), a given change in dynamic input results in a large activity change. With a larger static input (2), the dynamic component is shifted toward saturation and results in a smaller activity change. (b) During a task that requires detection of perturbation direction, noise forces the system to define thresholds (dashed lines) before a response decision is made. A smaller static component in Ia firing (1) implies that the dynamic component is greater and more easily distinguishable from noise, resulting in a faster response than that with a higher static component (2).

large errors will be detected, and the system will be insensitive to the kinds of errors that occur under normal conditions.

The following equation expresses the dynamics of χ used in the model:

$$\frac{d\chi}{dt} = (1 - \chi) - \chi R \tag{19}$$

where R is a source of inhibition that causes χ to decrease. In the absence of this inhibition χ grows to a value of 1. The formulation of explicit equations governing R is a task for future research. The control of this parameter may involve numerous central and peripheral factors. The three rules listed above are a starting point. Their translation into a mathematical formulation of neural mechanisms is not necessary to demonstrate some of their behavioral consequences. In the simulations below, the value of R is set in accordance with these rules and reported in the corresponding figure captions. A key condition used below, where R is set high to reduce the gain χ, is during vibration of muscle tendons. Such vibration is proposed to drive the system into a state where dynamic sensitivity is increased.

The fusimotor gating scheme described above is proposed primarily on functional grounds—it improves the system's performance during fast movements, and helps it to reproduce several psychophysical effects described below. Direct physiological and anatomical evidence for the mechanism is lacking, although support is provided by studies of "fusimotor set" during various movement scenarios. For example, it has been reported that during slow movements spindle activity is dominated by static fusimotor activity, whereas for movements faster than 0.2 resting lengths per second, spindles are dominated by velocity sensitivity (Prochazka, Stephens, & Wand, 1979). These results provide indirect support for rules 1 and 2, above. Prochazka, Hulliger, Trend, and Dürmüller (1988) provides some evidence for the third rule with the observation that during sudden imposed movements, dynamic fusimotor activity is high, while static activity is reduced. Dynamic fusimotor activity increases the system's sensitivity to imposed velocity errors.

Gating the Gain of Load Compensation

Consider the scenario of a quadruped raising itself off the ground and note that quadrupeds do not tonically support themselves in the gravity field by muscular action. Rather, muscular action is used only during the lifting phase, after which most of the weight is supported by the legs acting as stilts. During the lifting phase, contraction of the load-bearing muscles (extensors) is strongly opposed by the body's weight, requiring a large force to be generated by these muscles. This suggests that the gain of the load-compensation mechanism is increased during the lifting phase and decreased again once the body has been lifted onto its stilts. The lifting state is signaled by a conjunction of highly excited Golgi tendon organs and spindle receptors, and IaIb interneurons (Baldissera, Hultborn, & Illert, 1981) may detect this conjunction if their activity is contingent on the simultaneous input from Ia and Ib afferents.

This motivates the introduction of the following hypothesis. As the body is being lifted, the large muscle tensions excite Golgi tendon organs and the large position errors excite spindle receptors. This activates IaIb interneurons, which open a high-gain force accumulator. In the model, this function may be performed by the SFV

if the κ_i parameter of the load-bearing muscle is increased by Ia/b input. During the lifting phase, this high-gain mechanism helps to generate the large forces needed to lift the body. Once an upright position has been reached and the load has been transferred from the muscles to the column of bone, Golgi input to Ia/b interneurons disappears, and the SFV gain is again reduced to a modest value.

Vibration of an active load-opposing muscle may induce a state similar to that during the lifting stage because it significantly excites both spindle receptors and Golgi tendon organs (Burke, Hagbarth, Löfstedt, & Wallin, 1976a). Thus, it may also activate the Ia/b interneurons and cause high-gain SFV integration. Thus, we postulate that vibration increases the gain on the SFV integration of the vibrated spindle, changing the κ_i parameter (see Equation 16) of the vibrated muscle i. In our simulations, we changed κ_i from its normal value of 1 to a value of 400.

SIMULATIONS

This section describes a series of simulations reproducing psychophysical phenomena that illustrate different operating modes of the cortico-spinal trajectory generator.

Control of Fast versus Slow Movements: Response to Elastic Loads

In an attempt to understand the nature of the descending command underlying voluntary movement, Feldman et al. (1995) examined the differences between movements performed freely and those performed against an elastic load produced by a servomechanism programmed to behave like a linear spring. The subjects were asked to make reaching movements without visual feedback and instructed "not to correct arm deflections in case of perturbations." In control trials, subjects performed the movements with a mean movement time of about 100 msec, with the usual bell-shaped velocity profile and with minor oscillations around the endpoint. In test trials, a servomechanism applied force to the arm in a direction opposite to the movement direction and with a magnitude proportional to the displacement from the initial starting position. The typical force was 80 to 90% of the voluntary maximum for a given subject. During these trials, the movement stopped significantly before the target was reached and at about the same time that peak velocity was attained in the control movement. When the servo disengaged, the arm rapidly swung to the same position as that attained in the control movements. A linear velocity feedback was used to dampen endpoint oscillations.

Feldman et al. (1995) interpreted these results as support for the hypothesis that the descending motor command shifts the equilibrium point of the limb so rapidly that this shift stops well before the movement ends, in particular, at about the time that peak velocity is reached.

As discussed above, during fast movements the model reduces the influence of static feedback signals on trajectory generation. This frees the OPV command to shift to its final target value well before the movement completes, and in the extreme case of the fastest ballistic reaches, this shift completes before the arm overcomes inertia and begins to move. One may thus be tempted to describe the model's operation in this case as "spring-to-endpoint" movement. However, at these high speeds, the launching and braking pulses dominate the descending command, and the system's operation is better described as velocity control. Regardless, for the very fast movements (100 msec) performed by the subjects of Feldman et al. (1995), one may expect that static feedback has been reduced, and the OPV shift occurs much faster than the actual overt movement.

Figure 5 compares the data of Feldman et al. (1995) with simulations generated by the model. The servo action was simulated by augmenting Equation 1 as follows:

$$\frac{d^2p_i}{dt^2} = \frac{1}{I}\left[M(c_i, p_i) - M(c_j, p_j) + E_i - 4(0.5 - p_i) - V\frac{dp_i}{dt}\right] \tag{20}$$

and no damping action was provided. As in the data, the simulated loaded movement stops at about the same time that the control movement reaches its velocity peak, and the same target is reached when the servo disengages.

Postural versus Compliant Operation: Effects of Transient Perturbations

In the model, there are two kinds of influences on the descending command to alpha motor neurons (OFPV). Postural mechanisms work to maintain the limb in a centrally determined position; these mechanisms include DVV integration, SFV and IFV feedback loops, the stretch reflex, and spring properties of muscles. At the same time a compliance mechanism, the PPV-OPV pathway, releases tension on the limb by changing the OPV component of the descending command toward the actual position of the limb. The way in which these opposing influences interact is demonstrated by the following simulation.

The limb starts at a central TPV position with a positive GO signal, and a transient perturbation is applied. This perturbation exerts a force, which is a bell-shaped function of time, pulling the limb into extension. At the same time that the perturbing force disappears, the GO signal is shut off. The result, shown in Figure 6a, is a brief

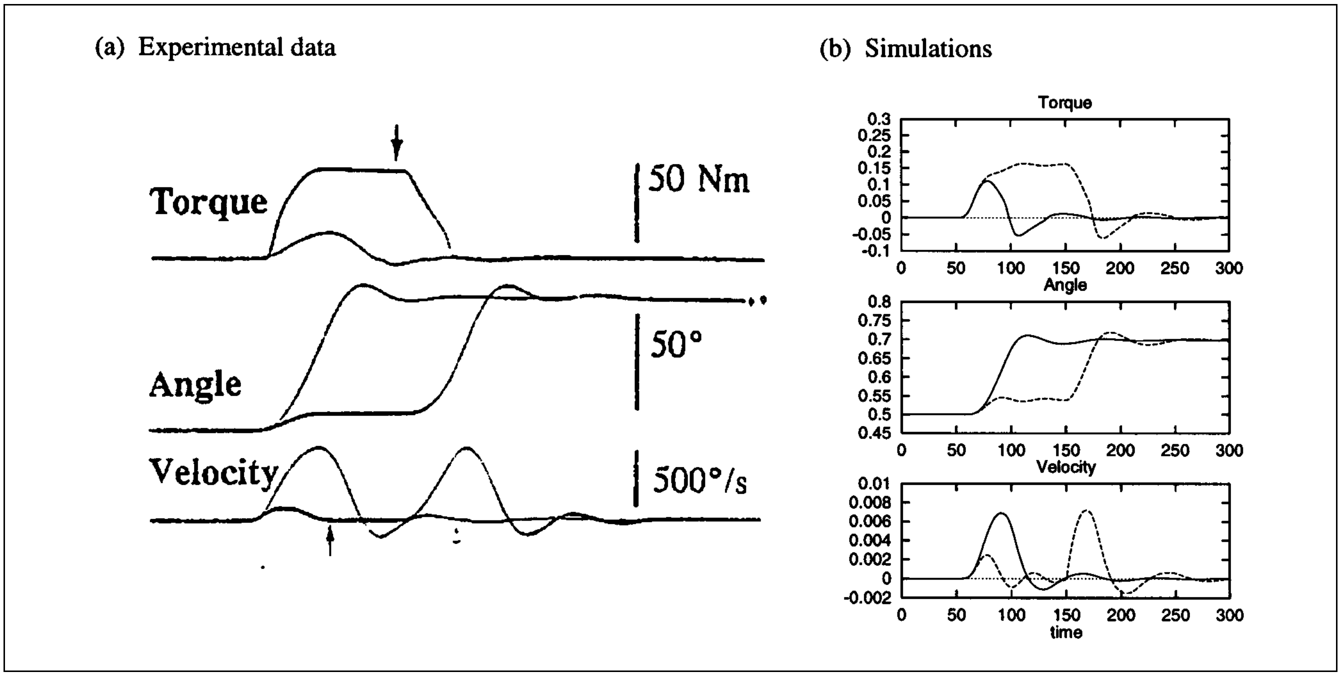

Figure 5. Simulation of the elastic load paradigm of Feldman et al. (1995). (a) Experimental data. The top arrow indicates the time when the servo action releases in a load trial. The lower arrow indicates the end of movement in a loaded trial. (b) Simulation results. The servo action was simulated by adding a force of $4(0.5 - p_1)$ to the limb dynamics Equation 1. This force was shut off at time $t = 150$. The GO signal scalar was set at $g^{(0)} = 0.7$ and static sensitivity reduced by setting $R = 1$. The simulated torque, angle, and velocity traces for the control movement are shown as solid lines; the same variables for the perturbed movement are shown as dashed lines.

extension of the limb followed by a return movement that does not quite reach the starting target position. The return movement illustrates the action of the postural mechanisms such as DVV integration and the spring property of the muscles. At the same time, the residual "endpoint error" illustrates the compliant influence of the PPV-OPV pathway. Because of this pathway, the OPV was drawn into extension, and shutting off of the GO signal prevented complete recovery.

This result is interesting because it is similar to the

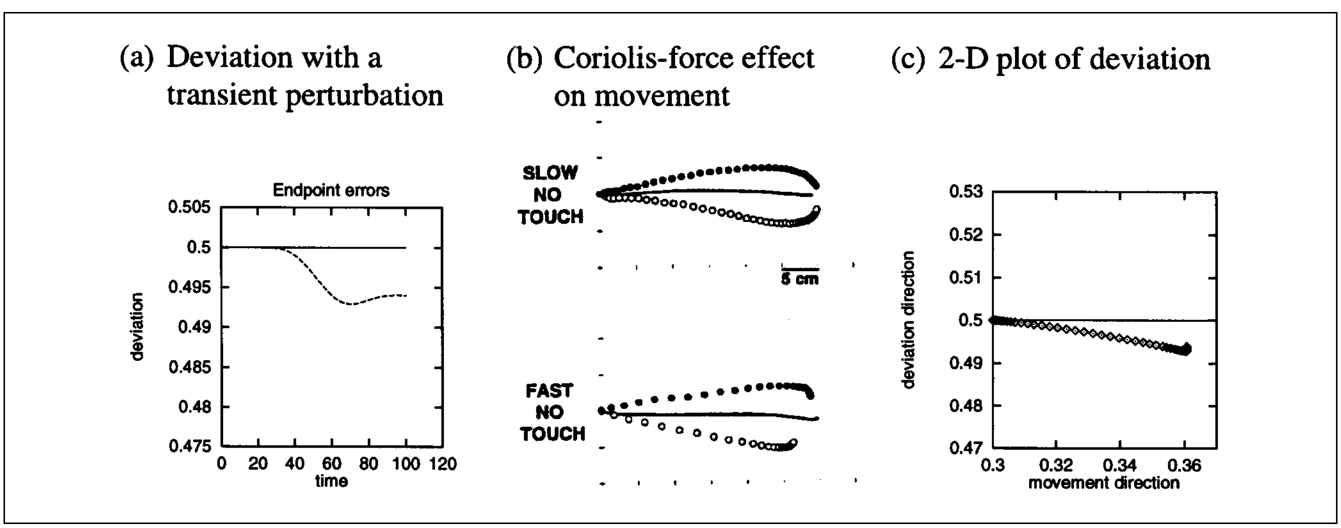

Figure 6. Simulation of the deviation in position caused by exposure to a force that was a bell-shaped function of time, peaking at $E_1 = 0.0055$. The GO signal was set at 0.1, and shut off at the same time that the force decayed back to zero. The moment of inertia was reduced to $I = 100$. (a) Plot of the position over time. (b) Data from Lackner and DiZio's (1994) Coriolis-force experiment, showing the prerotation movement (solid line), the first movement after rotation has started (open circles), and the first movement after rotation has stopped (filled circles) showing the after-effects of adaptation. (c) Plot of the simulation shown in (a) now presented in 2-D to facilitate comparison with the Coriolis-force data. The y-coordinate (deviation direction) is taken from the data shown in (a). The x-coordinate (movement direction) starts at 0.3 and is incremented by a step proportional to the magnitude of the bell-shaped force applied to the deviation direction.

endpoint errors observed during voluntary reaches made in a Coriolis force field (Lackner & DiZio, 1994). In a rotating room such as that used by Lackner and DiZio, a perturbing force is exerted upon the arm in a direction perpendicular to the direction of movement and of a magnitude proportional to the movement speed. When the arm stops moving, the force disappears. When first exposed to these conditions, subjects show curved trajectories whose endpoints deviate from the target position when movement terminates. This occurs both when contact is made with the surface upon which the target was displayed and when the arm is held above the surface (although the endpoint errors are smaller in the latter case). See Figure 6b for an example of such endpoint errors.

That trajectories are curved is expected purely due to the dynamics of the situation, on the assumption that feedback compensation is partial and delayed and that no feedforward compensation has yet been learned. Because subjects were instructed to "reach and touch the location of the target in one continuous natural movement without stopping" and were asked not to make voluntary corrective movements afterward, the GO signal is shut off as appropriate for an unperturbed movement. If the descending command were a purely feedforward kinematic equilibrium point command, one would expect it to move to the target just as it would in an unperturbed movement, and spring properties to bring the endpoint to the target with normal accuracy. Thus, one would not expect any endpoint errors greater than those normally observed to remain after external forces have disappeared. That endpoint errors occur has been taken as evidence against equilibrium point theories.

However, if one adds the assumption that movement is influenced by peripheral feedback, these results are not so surprising. Feedback could produce two kinds of results. A feedback positional compensation scheme with low gain and some lag would move the equilibrium point in the direction *opposite* to the load, whereas a system for complying with external forces would move it in the *same* direction as the load. The data support the latter, which is consistent with our hypothesis of a PPV-OPV pathway that allows compliance with external demands. Our simulation in Figure 6a is analogous to the effect of the perturbing Coriolis force on the direction perpendicular to the direction of movement. Along this direction, the target is constant, and the perturbing force is bell-shaped after the bell-shaped velocity profile along the movement direction. Figure 6c replots the same simulation in 2-D to facilitate comparison with the data.

Although subjects consistently exhibit the above-mentioned effects when first placed in a Coriolis field, they quickly adapt to the unusual force environment and exhibit straight movements that accurately reach the target (Lackner & DiZio, 1994; DiZio & Lackner, 1995). When the force field disappears after the room has stopped rotating, the subjects show opposite and equal aftereffects, including both curvature components and endpoint errors. Interestingly, whereas the endpoint error aftereffects are shown to transfer to the arm that made no movements during rotation, trajectory curvature aftereffects do not (DiZio & Lackner, 1995). This suggests a distinction between the mechanisms of adaptation that correct for kinematic versus kinetic errors.

The present model does not address such adaptation, although some of these effects may be generated if it is embedded within the DIRECT model of motor equivalent reaching and motor learning (Bullock, Grossberg, & Guenther, 1993), which extends the VITE model in another direction to learn spatial-to-motor coordinate transformations and to carry out reaches with a redundant arm (See "Discussion," below).

Active versus Passive Operation: Tonic and Antagonist Vibration Reflexes

The above simulation demonstrates how the system's active and passive modes of operation (controlled by the GO signal) help to reproduce errors seen in movements made in a Coriolis field. This section illustrates the difference between the states of active load-compensation and passive compliance with loads (controlled by the SFV integration parameter b) by comparing two different effects of muscle tendon vibration.

Tonic Vibration Reflex

When low-amplitude vibration of high frequency is applied to the muscle tendon, several sensory receptors are highly excited, including primary and secondary spindle afferents (Burke, Hagbarth, Löfstedt, & Wallin, 1976a, 1976b; Roll & Vedel, 1982). The effects of such vibration vary from subject to subject and depend in part upon the contraction state of the vibrated muscle.

The most immediate motor effect of muscle tendon vibration is a slow, continuous contraction of the vibrated muscle. This so called tonic vibration reflex (TVR) is observed when subjects are maintaining posture against gravity and does not occur when the vibrated arm is relaxed (Hagbarth & Eklund, 1966). In the model, the TVR can occur through several independent pathways: First, modest contraction is expected due to the stretch reflex (Equation 18). Depending on the balance of the response from primary versus secondary spindles, a second pathway may involve the IFV, which excites the agonist OFPV population and thus also causes muscle contraction (Equations 14 and 17). However, the major component of the reflex is generated in the model through the static force vector (SFV).

When the limb is maintaining posture against gravity, the b parameter in the SFV Equation 16 is positive. This implies that vibration and spindle excitation will lead to integration at the SFV cells. This integration produces the

type of slow continuous contraction that is seen during the tonic vibration reflex, as shown in Figure 7. When vibration stops, the arm returns toward its initial position due to the inhibition of the SFV by the antagonist spindles and the consequent reduction of the alpha motor neuron command.

In simulating vibration, a term is added to the input of the spindle saturation function, and so Equations 10 and 15 become, respectively,

$$s_i^{(1)} = S\left(\theta[\gamma_i^S - p_i]^+ + \phi\left[\gamma_i^D - \frac{dp_i}{dt}\right]^+ + \varphi^{(1)} vib_i\right) \quad (21)$$

and

$$s_i^{(2)} = S\left(\theta\left[\gamma_i^S - p_i\right]^+ + \varphi^{(2)} vib_i\right) \quad (22)$$

where $\varphi^{(1)} = 0.01$ is the primary afferent sensitivity to vibration, $\varphi^{(2)} = 0.01$ is the secondary afferent sensitivity, and vib_i is proportional to the vibration frequency applied to muscle i. Note that because vibration drives spindles to abnormally high activity levels, close to saturation, it dominates the other sources of excitation. It is postulated that during vibration, the system enters a state analogous to the set adopted during exposure to unexpected perturbations (e.g., Prochazka, 1992). Thus, during vibration, static sensitivity is reduced by setting $R > 0$ (see Equation 19). This means that vibration causes the gating parameter χ to be reduced below 1 and the system to shift into the dynamically sensitive state.

Antagonist Vibration Reflex

As mentioned above, the tonic vibration reflex occurs only when the limb is actively maintaining posture against gravity. When the limb is relaxed, vibration produces the opposite result; namely, EMG activity in the antagonist of the vibrated muscle (Gilhodes, Roll, & Tardy-Gervet, 1986). This effect is called the antagonist vibration reflex (AVR).

In the context of the model, the difference between the TVR and the AVR may be due to two factors. First, a central variable (e.g., h in Equation 16) may shut off the load compensation mechanism that underlies the TVR. Second, relaxation of the muscle may render the Golgi tendon organs much less responsive to vibration, thus failing to excite the IaIb interneurons and activate the high-gain force accumulation described above.

Below, the AVR is simulated by setting the SFV integration rate h to zero and keeping $\kappa_i = 1$. Without the growth of the static force vector, the dominant effect of biceps vibration is stimulation of the primary afferents that project to the PPV. Because spindle afferents signal stretch of the muscle from which they project (McCloskey, Cross, Honner, & Potter, 1983), this produces a percept of extension. Because the system is in a relaxed state, this percept induces activity changes attempting to comply with imposed movement (through the PPV-OPV pathway). The result is EMG activity in the antagonist and generation of force into extension, as shown in Figure 8.

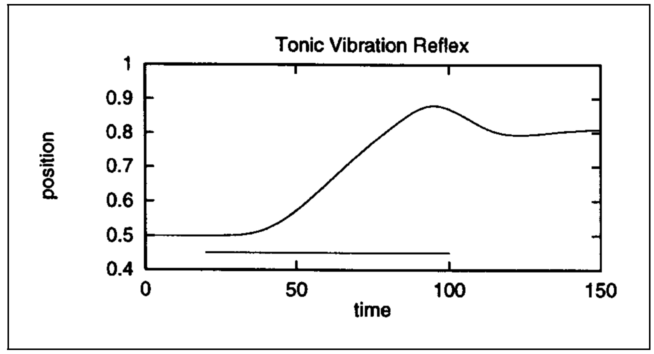

Figure 7. Simulation of the tonic vibration reflex. Vibration was applied by setting $vib_1 = 0.2$ during the time period indicated by the horizontal line. The limb was actively resisting gravity (i.e., h = 0.025, and κ_I was increased to 400).

The mechanisms by which the model generates the TVR and AVR suggest testable predictions. Because the TVR is mediated through a pathway that acts only through alpha motor neurons, one should expect it to cause unloading of the spindles in the vibrated muscle. This is indeed observed in vivo (Burke et al., 1976b) as a decreased response to vibration during the TVR. In contrast, because the AVR involves a pathway through the OPV, one should not expect unloading of the spindles antagonistic to the vibrated muscle, because both the intrafusals and extrafusals receive the OPV command. In addition, although the TVR appears to survive decerebration, at least in the cat (Matthews, 1966) (which suggests that a subcortical SFV may project to subcortical or spinal regions in addition to the cortical OFPV), the AVR is expected not to.

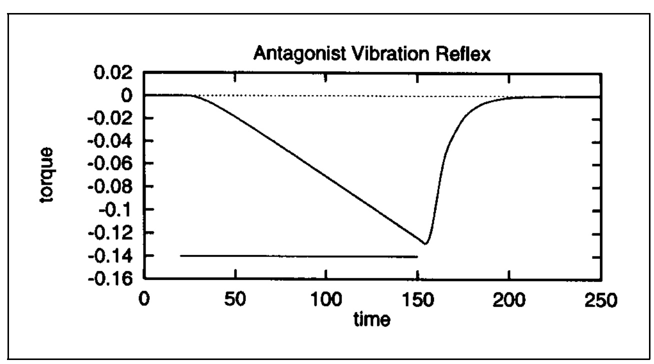

Figure 8. Simulation of the antagonist vibration reflex. Vibration was applied by setting $vib_1 = 0.2$ during the time indicated by the horizontal line. The limb was relaxed (i.e., h = 0.0) and held at a position of 0.5. The solid line shows the value of the alpha motor neuron activation α_1; the reduction of this variable implies that forces are exerted into extension.

Position versus Velocity Feedback: Vibration-Induced Proprioceptive Illusions

With the assumption that proprioception is based in part on peripheral feedback originating with spindle receptors, one would expect proprioceptive illusions to occur when the activity of these receptors is stimulated artificially while vision is removed as an alternative information source. Such illusions have indeed been consistently observed when tendon vibration is applied to muscles. The resulting effects include misperceptions of position and illusions of movement (Craske, 1977; Gilhodes et al., 1986; Goodwin, McCloskey, & Matthews, 1972a, 1972b; McCloskey, 1973) and even *visual* illusions (Lackner & Levine, 1978; Lackner & Taublieb, 1984) under degraded visual conditions. This section reviews these data and demonstrates how the model is capable of reproducing some key documented effects.

Static and Dynamic Proprioception Illusions

When tendon vibration is applied to the biceps muscle of an immobile arm, subjects report a perception of movement into extension. Conversely, a percept of flexion is induced when vibration is applied to the triceps. These effects are consistent with the hypothesis, expressed by Equation 7 above, that an internal representation of limb position is obtained by subtracting from the efference copy of a motor command the error signal from muscle spindles. For example, when vibration is applied to the biceps tendon, activated flexor spindles inhibit the flexor component of the PPV while exciting the extensor component. Again, vibration causes $R > 0$ and reduction of the fusimotor gain χ (see Equation 19), thereby putting the system in a mode of dynamic proprioception, and thus the illusion is one of movement. In cases where χ is not significantly reduced, the result is a perception that the arm is more extended than it is in reality, but not a percept of movement. Indeed, some subjects report such a static illusion, while others report a dynamic illusion of movement (Goodwin et al., 1972b). It may be postulated that the difference between these subjects is the extent to which their fusimotor activation is affected by the vibratory stimulus. Figure 9 shows simulations of both kinds of illusions.

Illusions during Vibration of Agonist and Antagonist Muscles

When both the biceps and triceps are vibrated simultaneously, human subjects report a perception of movement that depends upon which muscle is vibrated with the higher frequency (Gilhodes et al., 1986). For example, if the biceps is vibrated at a higher frequency than the triceps, the illusion is one of extension. The speed of the illusory movement depends upon the difference between the two vibration frequencies. Figure 10a shows a plot of the data (from Table 2 of Gilhodes et al., 1986) and Figure 10b shows analogous results generated by the model.

When fusimotor gain χ is reduced, the model is capable of reproducing these results due to the PPV computation mechanism (7) and the spindle saturation function (11), which together implement a rectified difference of two saturating signals.

Illusions during Obstructed Tonic Vibration Reflex

A classic and quite striking perceptual phenomenon, first reported by Goodwin et al. (1972a, 1972b) occurs when a tonic vibration reflex is induced in human subjects, producing movement, and then is obstructed by an obstacle. With biceps vibration, the perceptual effect begins as flexion that lags the actual TVR flexion (some subjects report a brief sensation of extension before the TVR movement begins). Then, when the obstacle is encountered, the percept reverses into extension. When vibration ceases, the perceived position of the arm quickly

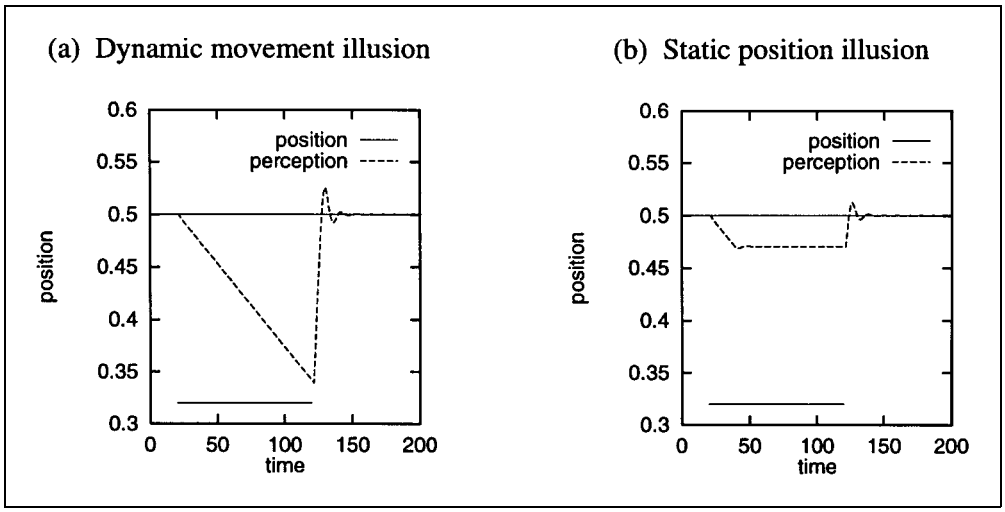

Figure 9. Simulations of vibration-induced proprioceptive illusions. In both plots, vibration of $vib_1 = 0.3$ was applied during the time indicated by the horizontal line. (a) Dynamic illusion obtained when χ is significantly reduced by vibration ($R = 1$ during vibration). (b) Static illusion obtained when χ is less reduced ($R = 0.05$ during vibration). In both cases, the limb was relaxed (i.e., $b = 0, g^{(0)} = 0$) and held at the central position.

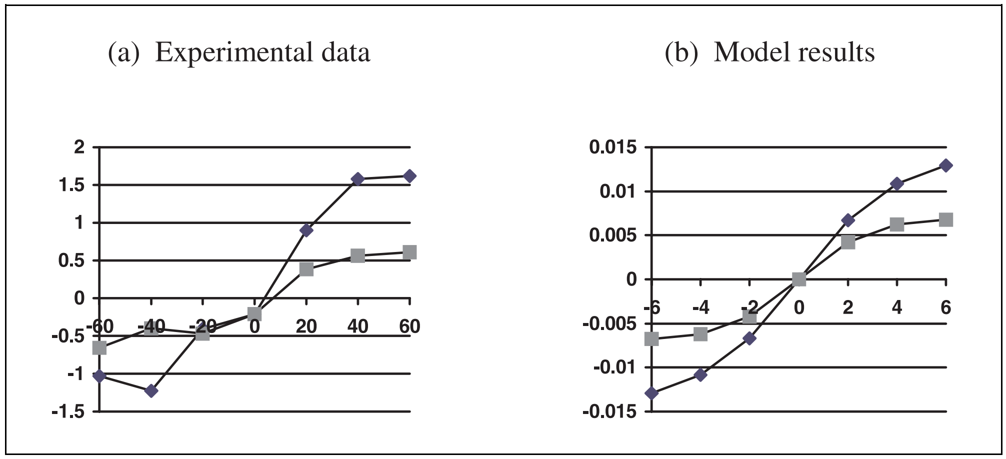

Figure 10. Effects of vibration of both muscles at different frequencies. (a) Data from Gilhodes et al. (1986). The abscissa shows the difference between the vibration frequency applied to the biceps minus the frequency applied to the triceps, in hertz. Diamonds indicate data points for trials where the lower vibration frequency was 20 Hz, and squares indicate where the lower frequency was 40 Hz. The speed of illusory movement is shown in degrees per second. (b) Analogous data generated by the model, with the abscissa showing the value of $vib_1 - vib_2$ and the ordinate showing the perceived speed in fractions of the full position range per time step. Parameter R was set to 1 during vibration. Diamonds indicate data points for trials with a lower vibration of 2.0, and squares indicate those with a lower vibration of 4.0. Note that these vibration frequencies are much higher, relative to normal spindle firing, than the vibrations applied experimentally. This is unlike other simulations of vibration effects and was necessary to make the saturation effect more visible. Consequently, the perceived speed is much higher in the simulation: Assuming that the position range 0 to 1 represents 180° and that 10 time steps equal 1 sec, a perceived speed of 0.015 translates to 27°/s.

becomes accurate—this is sometimes accompanied by an inadvertent movement of the vibrated arm toward the previous, illusory position. Figure 11a shows an example of the movement and the perceived position, the latter indicated by the subjects using their other arm.

The model allows the illusion to be explained as follows: First, vibration of the biceps causes an extension signal to arrive at the PPV. This is brief, however, because soon the arm begins to flex due to the tonic vibration reflex through the SFV. This flexion movement stretches the spindles in the triceps, which signal flexion to the PPV. The two conflicting signals subtract at the PPV, resulting in a percept of flexion that lags the actual flexion by some amount. When the obstacle prevents further flexion, the triceps spindles are no longer stretched and the only remaining signal to the PPV is the signal of extension carried by the Ia fibers from the biceps, excited by vibration. After vibration stops, the system receives accurate peripheral information, and because χ has returned to 1 once vibration ceased, it can reconstruct a correct PPV pattern based on the static information now available. This may sometimes be accompanied by a short return movement as the built-up SFV activity is inhibited by the sudden activation of the antagonist secondary spindle as χ returns to 1 (see Equation 16).

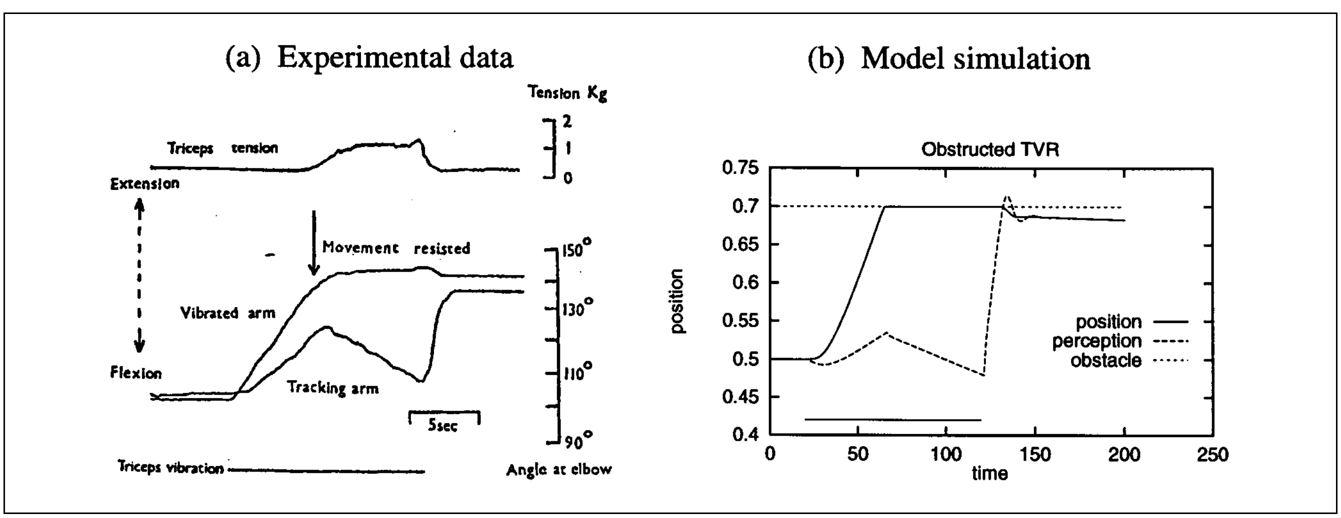

Figure 11. Obstructed tonic vibration reflex. (a) Figure 3 from Goodwin et al. (1972b). The plot shows the movement and illusion resulting from triceps vibration. Note that this figure plots position with extension in the positive direction and flexion in the negative, unlike the other figures used here. (b) Simulation generated by setting $vib_1 = 0.25$ and $R = 1$ during the period indicated by the horizontal line, with load compensation on ($b = 0.02$). The mass of the limb and the PPV-OPV gain were reduced to $I = 10$ and $\eta = 0.4$.

In the model, the effect is generated in the same way as the TVR of Figure 7, only an obstacle is introduced, which prevents the position from exceeding a flexion value of 0.7. As simulated in Figure 11b, model behavior closely emulates the data, including the brief percept of extension, followed by a percept of flexion that lags the actual movement, followed by an illusion of extension, and finally the rapid accurate PPV computation accompanied by a small return movement.

Some intersubject variability can be simulated by the model as well. Specifically, during the actual arm movement, some subjects indicate a position that lags the actual position, but the lag does not increase over time (Goodwin et al., 1972b). After the obstacle is reached, some subjects report only a brief illusion of movement that quickly stops at a stable, albeit inaccurate, position. Both these effects can be produced in the model if the χ parameter is not sufficiently reduced during vibration, as shown in Figure 12.

Reaching Inaccuracies under Vibration

If the central representation of current limb position (PPV) is based in part on peripheral feedback from muscle spindles, and if this representation is used in computing the planned movement (DV), one would expect tendon vibration to disrupt reaching movements in predictable ways. For example, when muscle vibration causes an illusion that the arm is more flexed than it actually is, reaching movements into flexion should exhibit undershoots. In the model, this occurs because the DV is prematurely driven to zero by a PPV that is misrepresenting the actual limb position.

When humans perform reaching movements while their muscle tendons are vibrated, undershoots in reaching are observed (Capaday & Cooke, 1981, 1983). The typical effects, shown in Figure 13a, were obtained when subjects made alternating flexion and extension movements, without visual feedback, while their triceps tendon was vibrated. Note that the movements show undershoots in the flexion phase but not in the extension phase. This asymmetry in the effects of vibration on reaching movements has been consistently observed in similar studies and has led to the conclusion that, during movement, the motor system is only attending to the feedback information coming from the muscle that is being stretched (Capaday & Cooke, 1983). This makes sense when one considers that the spindles in the contracting muscle are more likely to become unloaded and are thus a less reliable source of feedback information.

Figure 13b shows a simulation generated by the model. The model generates the same kind of undershoots during the flexion phase. The magnitude of these undershoots in the simulation is smaller, as a percentage of the total movement extent, than those observed in the data. This might indicate other influences upon the PPV and/or the movement command or may simply be a consequence of the mathematical simplifications used above in formalizing the neural circuit.

Capaday and Cooke (1981) also showed that when subjects are allowed visual feedback of their arm, the effects of vibration disappear, and movements are made accurately regardless of which muscle is vibrated. Again, this makes sense in the context of the model if it is augmented by visually sensitive mechanisms of the DIRECT model (Bullock et al., 1993). Then visual information, if available, dominates the proprioceptive feedback in the computation of the PPV. Therefore, one would expect

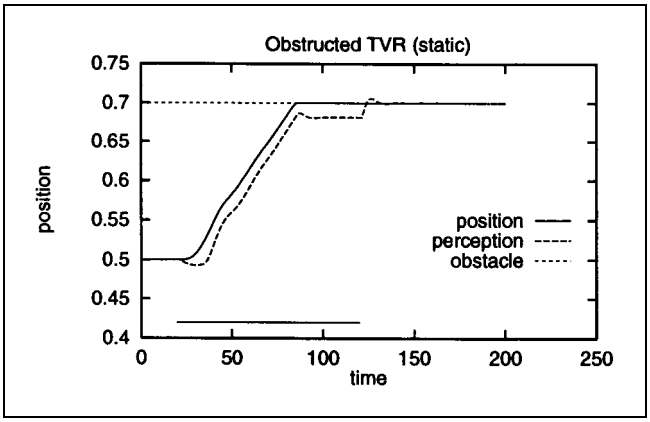

Figure 12. Static version of the obstructed TVR illusion. Unlike the simulation shown in Figure 11b, the plot shown above was obtained with $R = 0.05$ during the period of vibration.

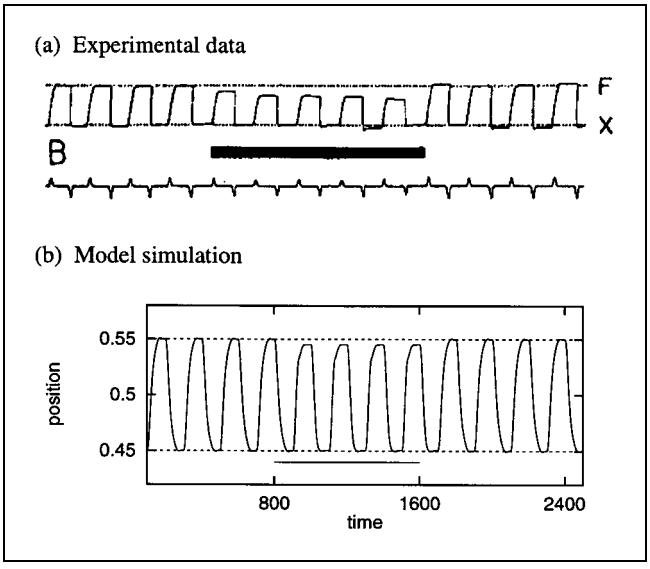

Figure 13. Reaching movements performed with vibration. (a) Data from Capaday and Cooke (1981) on alternating reaching movements performed with triceps vibration. The solid line indicates position and dotted lines indicate the targets. The solid bar shows the time of vibration. (b) Simulation of reaching movements made between the targets shown by dotted lines, with GO = 0.5, and $b = 0$. During the period of vibration, indicated by the horizontal line, $vib_1 = 2$ and $R = 1$. The moment of inertia was set to $I = 50$ to reduce oscillations.

the misleading spindle information to be ignored in the DV computation and the reaching movements to be performed accurately.

DISCUSSION

In order to perform voluntary goal-directed reaching, the motor system must generate movement commands appropriate for both the internal demands (target and speed of movement) and external conditions (loads and obstacles). This means that central and peripheral signals must be integrated in the nervous system and together used to guide the development of contraction in the muscles. Bullock et al. (1998) have described a circuit model that performs such integrated control of voluntary movements and proposed how its elements correspond to neurophysiologically identified cortical and subcortical cell types. However, the operation described therein is not appropriate for all movement contexts. For example, for slow precise movements, a representation of limb position derived in part from peripheral feedback information is desirable, but such feedback may be undesirable during very fast movements when lags render the information useless and even detrimental to stability. The motor system must allow modification of its operating mode toward one appropriate to the given movement context. Such modification may be implemented through automatic or volitional gating mechanisms that control the balance of various influences acting upon the movement command.

This report discusses such influences, which may be summarized as follows:

1. *Passive versus active operation.* The balance between the response to internal versus external demands is controlled by two separate gating operations. The GO signal controls the speed of voluntary movement, as well as the effort with which forces are exerted against obstructions and the speed of the response to perturbations. The SFV integration rate (parameters h) controls the gain of the load-compensation machinery.

2. *High-gain versus low-gain force generation.* The magnitude of forces exerted against perturbing loads is also controlled through muscle-specific gains on SFV integration (parameter κ_i). During normal operation, this gain is modest, but it is increased during tasks that demand large force generation such as during the process of lifting a body off the ground.

3. *Fast versus slow movement.* During fast movements, static positional error signals are outdated and potentially destabilizing. Thus, the system reduces the sensitivity of muscle spindles to stretch by reducing the activation of static gamma motor neurons. This shifts the system from a feedback position controller during slow movements to a feedforward trajectory generator with feedback velocity compensation during fast movements.

4. *Static versus dynamic sensitivity.* When fast responses are desired to perturbations from unpredictable directions, the system changes the balance of static versus dynamic information in the feedback streams. This is also controlled by reduction of the activation of static gamma motor neurons, leaving more of the firing range of Ia fibers for the dynamic velocity information.

Still other kinds of gating seem to exist in vivo. One example is stiffness control, which is accomplished in part by cocontractions of antagonistic muscles. Although the role of higher brain centers in stiffness control has not been definitively established (see Smith, 1996, and associated commentaries), there have been many observations of systematic variations in cocontraction as a function of variables such as subject age and load size (Gachoud, Mounoud, Havert, & Viviani, 1983) and the frequency of perturbations to posture (Humphrey & Reed, 1983). The FLETE model (Bullock & Grossberg, 1989, 1990, 1992; Bullock & Contreras-Vidal, 1993; Bullock, Contreras-Vidal, & Grossberg, 1993) describes how spinal circuits would enable a descending cocontractive signal to control stiffness independent of position. The present model is consistent with such a spinal circuit model.

Additional Psychophysical Phenomena Relevant to the Model

The computation of the Perceived Position Vector (PPV) from central and peripheral information allows the potential explanation of several additional psychophysical phenomena involving tendon vibration. One is the report by Craske (1977) that when vibration is applied to the biceps while the arm is passively moved into full extension, subjects report perceptions of hyperextension. Although no actual pain is felt by these subjects, they experience the very unpleasant sensation that their arm "is bent backward" or "being broken." These results led Craske (1977) to conclude that the computation of position involves an extrapolation based on central and peripheral signals, operating on the previously calibrated natural position domain. In the context of the model, one may suppose that normal joint angles are coded by a central range of firing frequencies of the cells that represent the Perceived Position Vector. This would assist PPV accuracy by keeping computations away from nonlinear extremes of cell activity. Vibration applied to an extending biceps may then push these cells to their extremes and be interpreted as hyperextension of the elbow.

The present model is intended to fit within a larger theory of motor control, which includes the DIRECT model of motor-equivalent reaching and learning (Bullock et al., 1993). One focus of the DIRECT model is to analyze the way in which visual and somatosensory signals are combined in the construction of a spatial

representation of the PPV, which is used to compute a movement direction vector (DV) in spatial coordinates rather than in the motor coordinates used here for simplicity. The present model naturally fits within the DIRECT framework through the elaboration of the computations involving PPV, TPV, and DV. In brief, a PPV representation in joint coordinates can be used to update a visuo-spatial representation of end-effector perceived position.

With this in mind, one may begin to make sense of some remarkable illusions first reported by Lackner and Levine (1978). In these experiments, a small LED was attached to the finger of a human subject, who was placed in a completely dark room. The subject's relaxed arm was held immobile in a brace, and tendon vibration was applied to the biceps. The standard somatosensory illusions described above were observed. However, in addition to these, subjects reported *seeing* the movement of the LED in the direction consistent with extension of their elbow. In other words, the proprioceptive stimulation produced a visual effect, called the *oculobrachial illusion.*

Consideration of how the present model may be joined to DIRECT mechanisms offers some potential of explaining this effect. If visual and somatosensory signals combine in the computation of the PPV, the conscious interpretation of the result of this computation may ascribe the perceived movement to be due to a visual stimulus. When a single small light is visible in an otherwise dark room, it is often perceived to move around haphazardly as the eye jitters about. This autokinesis may result from a slight miscalibration of corollary discharge signals from extraocular muscles and retinal slip signals. In the oculobrachial illusion, the somatosensory illusion of movement passing through to the PPV may be enough to bias autokinesis in the direction consistent with arm extension, especially because the subjects are consciously aware that the LED is fixed to their finger.

Conclusions

Modulation of a cortico-spinal circuit model for trajectory generation and dynamics compensation with automatic and volitional mechanisms allows the system to achieve a high degree of task sensitivity. The model reproduces a number of illustrative psychophysical phenomena, including responses to elastic loads during fast movements, endpoint errors in Coriolis force fields, and several kinds of effects caused by muscle tendon vibration. The model realizes a set of functional hypotheses about flexible movement control, which enable it to unify neurophysiological, anatomical, and psychophysical data, within a computational framework. This developing theory can be extended in a number of directions. First, model cell populations may be unlumped toward a more detailed treatment of physiological phenomena such as recruitment gradients and distributed representations (see Bullock et al., 1998). Second, the model's trajectory formation circuit may be embedded within several theories that address sensorimotor transformations and multijoint control (Bullock et al., 1993; Jordan, 1990; Kettner, Marcario, & Port, 1993; Kuperstein, 1988; Mel, 1991). Finally, the model may be joined to VITE-like circuits that illustrate how more complex movement sequences are planned and executed with variable speed, size, and shape, as in the kinds of curved movements that are synthesized during handwriting (Bullock, Grossberg, & Mannes, 1992).

Appendix A. Model Parameters

Except where noted, all the simulations above use the following parameter settings: $I = 200$, $V = 10$, $\nu = 0.1$, $B^{(r)} = 0.1$, $\rho = 0.07$, $\theta = 0.7$, $\phi = 1.0$, $B^{(u)} = 0.01$, $\varepsilon = 0.01$, $C = 25$, $\eta = 0.7$, $\lambda = 10$, $\Lambda = 0.003$, $P = 0.0001$, $\delta = 0.1$, $h = 0.025$, $\kappa_i = 1$, $\psi = 15$, $R = 0$. The delay in feedback from spindles to central variables (PPV, SFV, and IFV) is controlled by the parameter τ, normally set at $\tau = 5$. Because a moderate-speed movement takes about 100 time steps in the model, the delay is approximately 5% of movement time. The adverse effects of larger feedback delays may be reduced by feedforward compensatory machinery in addition to the reduction of static sensitivity discussed above.

Acknowledgments

This research was supported in part by the Office of Naval Research (ONR N00014-92-J-1309, ONR N00014-93-1-1364, and ONR N00014-95-1-0409). The first author was also supported in part by the Defense Advanced Research Projects Agency (ONR N00014-92-J-4015), the National Science Foundation (NSF IRI-90-24877 and NSF IRI-90-00530), Fond pour la formation de Chercheurs et l'Aide à la récherche (FCAR 124-82-058-000), and the Medical Research Council (MRC 24-29-058-490).

Reprint requests should be sent to Daniel Bullock or Stephen Grossberg, CNS Department, Boston University, 677 Beacon Street, Boston, MA 02215.

REFERENCES

Alexander, G. E., & Crutcher, M. D. (1990). Preparation for movement: Neural representations of intended direction in three motor areas of the monkey. *Journal of Neurophysiology, 64,* 133–150.

Atkeson, C. G., & Hollerbach, J. M. (1985). Kinematic features of unrestrained vertical arm movements. *Journal of Neuroscience, 5,* 2318–2330.

Baldissera, A., Hultborn, H., & Illert, M. (1981). Integration in spinal neuronal systems. In V. B. Brooks (Ed.), *Motor control: Handbook of physiology,* Sect. 1, Vol. 2 (pp. 509–595). Bethesda, MD: American Psychological Society.

Bizzi, E., Accornero, N., Chapple, W., & Hogan, N. (1984). Posture control and trajectory formation during arm movement. *Journal of Neuroscience, 4,* 2738–2744.

Bullock, D., Cisek, P., & Grossberg, S. (1998). Cortical networks for control of voluntary arm movements under variable force conditions. *Cerebral Cortex, 8,* 48–62.

Bullock, D., & Contreras-Vidal, J. L. (1993). How spinal neural networks reduce discrepancies between motor intention and motor realization. In K. M. Newell & D. M. Corcos (Eds.), *Variability and motor control* (pp. 183–221). Champaign, IL: Human Kinetics Press.

Bullock, D., Contreras-Vidal, J. L., & Grossberg, S. (1993). Equilibria and dynamics of a neural network model for opponent muscle control. In G. A. Bekey & K. Y. Goldberg (Eds.), *Neural networks in robotics* (pp. 439–457). Boston, MA: Kluwer Academic.

Bullock, D., & Grossberg, S. (1988). Neural dynamics of planned arm movements: Emergent invariants and speed-accuracy properties during trajectory formation. *Psychological Review, 95,* 49–90.

Bullock, D., & Grossberg, S. (1989). VITE and FLETE: Neural modules for trajectory formation and postural control. In W. A. Hershberger (Ed.), *Volitional action* (pp. 253–297). Amsterdam: North Holland.

Bullock, D., & Grossberg, S. (1990). Spinal network computations enable independent control of muscle length and joint compliance. In R. Eckmiller (Ed.), *Advanced neural computers* (pp. 349–356). Amsterdam: North Holland.

Bullock, D., & Grossberg, S. (1991). Adaptive neural networks for control of movement trajectories invariant under speed and force rescaling. *Human Movement Science, 10,* 1–51.

Bullock, D., & Grossberg, S. (1992). Emergence of tri-phasic muscle activation from the non-linear activations of central and spinal neural network circuits. *Human Movement Science, 11,* 157–167.

Bullock, D., Grossberg, S., & Guenther, F. H. (1993). A self-organizing neural model of motor equivalent reaching and tool use by a multijoint arm. *Journal of Cognitive Neuroscience, 5,* 408–435.

Bullock, D., Grossberg, S., & Mannes, C. (1992). A neural network for cursive script production. *Biological Cybernetics, 70,* 15–28.

Burbaud, P., Doegle, C., Gross, C., & Bioulac, B. (1991). A quantitative study of neuronal discharge in areas 5, 2, and 4 of the monkey during fast arm movements. *Journal of Neurophysiology, 66,* 429–443.

Burke, D., Hagbarth, K., Löfstedt, L., & Wallin, B. G. (1976a). The responses of human muscle spindle endings to vibration of non-contracting muscles. *Journal of Physiology, 261,* 673–693.

Burke, D., Hagbarth, K., Löfstedt, L., & Wallin, B. G. (1976b). The responses of human muscle spindle endings to vibration during isometric contraction. *Journal of Physiology, 261,* 695–711.

Capaday, C., & Cooke, J. D. (1981). The effects of muscle vibration on the attainment of intended final position during voluntary human arm movements. *Experimental Brain Research, 42,* 228–230.

Capaday, C., & Cooke, J. D. (1983). Vibration-induced changes in movement-related EMG activity in humans. *Experimental Brain Research, 52,* 139–146.

Chapman, C. E., Spidalieri, G., & Lamarre, Y. (1984). Discharge properties of area 5 neurones during arm movements triggered by sensory stimuli in the monkey. *Brain Research, 309,* 63–77.

Cheney, P. D., & Fetz, E. E. (1980). Functional classes of primate corticomotoneuronal cells and their relation to active force. *Journal of Neurophysiology, 44,* 773–791.

Clark, F. J., Burgess, R. C., Chapin, J. W., & Lipscomb, W. T. (1985). Role of intramuscular receptors in the awareness of limb position. *Journal of Neurophysiology, 54,* 1529–1540.

Crammond, D. J., & Kalaska, J. F. (1989). Neuronal activity in primate parietal cortex area 5 varies with intended movement direction during an instructed-delay period. *Experimental Brain Research, 76,* 458–462.

Craske, B. (1977). Perception of impossible limb positions induced by tendon vibration. *Science, 196,* 71–73.

Crutcher, M. D., & Alexander, G. E. (1990). Movement-related neuronal activity selectively coding either direction or muscle pattern in three motor areas of the monkey. *Journal of Neurophysiology, 64,* 151–163.

DiZio, P., & Lackner, J. R. (1995). Motor adaptation to Coriolis force perturbations of reaching movements: Endpoint but not trajectory adaptation transfers to the nonexposed arm. *Journal of Neurophysiology, 74,* 1787–1792.

Evarts, E. V. (1968). Relation of pyramidal tract activity to force exerted during voluntary movement. *Journal of Neurophysiology, 31,* 14–27.

Evarts, E. V. (1974). Precentral and postcentral cortical activity in association with visually triggered movement. *Journal of Neurophysiology, 37,* 373–381.

Feldman, A. G., Adamovich, S. V., & Levin, M. F. (1995). The relationship between control, kinematic and electromyographic variables in fast single-joint movements in humans. *Experimental Brain Research, 103,* 440–450.

Fitts, P. M. (1954). The information capacity of the human motor system in controlling the amplitude of movement. *Journal of Experimental Psychology, 47,* 381–391.

Fromm, C., Wise, S. P., & Evarts, E. V. (1984). Sensory response properties of pyramidal tract neurons in the precentral motor cortex and postcentral gyrus of the rhesus monkey. *Experimental Brain Research, 54,* 177–185.

Gachoud, J. P., Mounoud, P., Havert, P., & Viviani, P. (1983). Motor strategies in lifting movements: A comparison of adult and child performance. *Journal of Motor Behavior, 15,* 202–216.

Georgopoulos, A. P., Ashe, J., Smyrnis, N., & Taira, M. (1992). The motor cortex and the coding of force. *Science, 256,* 1692–1695.

Georgopoulos, A. P., Caminiti, R., & Kalaska, J. F. (1984). Static spatial effects in motor cortex and area 5: Quantitative relations in a two-dimensional space. *Experimental Brain Research, 54,* 446–454.

Georgopoulos, A. P., Caminiti, R., Kalaska, J. F., & Massey, J. T. (1983). Spatial coding of movement: A hypothesis concerning the coding of movement direction by motor cortical populations. *Experimental Brain Research, (Suppl.) 7,* 327–336.

Georgopoulos, A. P., Kalaska, J. F., Caminiti, R., & Massey, J. T. (1982). On the relations between the direction of two-dimensional arm movements and cell discharge in primate motor cortex. *Journal of Neuroscience, 2,* 1527–1537.

Gielen, C. C. A. M., & Houk, J. C. (1987). A model of the motor servo: Incorporating nonlinear spindle receptor and muscle mechanical properties. *Biological Cybernetics, 57,* 217–231.

Gilhodes, J. C., Roll, J. P., & Tardy-Gervet, M. F. (1986). Perceptual and motor effects of agonist-antagonist muscle vibration in man. *Experimental Brain Research, 61,* 395–402.

Goodwin, G. M., McCloskey, D. I., & Matthews, P. B. C. (1972a). Proprioceptive illusions induced by muscle vibration: Contribution by muscle spindles to perception? *Science, 175,* 1382–1384.

Goodwin, G. M., McCloskey, D. I., & Matthews, P. B. C. (1972b). The contribution of muscle afferents to kinæsthesia shown by vibration induced illusions of movement

and by the effects of paralysing joint afferents. *Brain, 95,* 705–748.
Hagbarth, K., & Eklund, G. (1966). Motor effects of vibratory muscle stimuli in man. In R. Granit (Ed.), *Muscular afferents and motor control* (pp. 177–186). Stockholm: Almquist & Wiksell.
Humphrey, D. R., & Reed, D. J. (1983). Separate cortical systems for control of joint movement and joint stiffness: Reciprocal activations and coactivation of antagonist muscles. In J. E. Desmedt (Ed.), *Motor control mechanisms in health and disease* (pp. 347–372). New York: Raven.
Jordan, M. I. (1990). Motor learning and the degrees of freedom problem. In M. Jeannerod (Ed.), *Attention and performance XIII: Motor representation and control* (pp. 796–836). Hillsdale, NJ: Erlbaum.
Kalaska, J. F., Cohen, D. A. D., Hyde, M. L., & Prud'homme, M. J. (1989). A comparison of movement direction-related versus load direction-related activity in primate motor cortex, using a two-dimensional reaching task. *Journal of Neuroscience, 9,* 2080–2102.
Kalaska, J. F., Cohen, D. A. D., Prud'homme, M. J., & Hyde, M. L. (1990). Parietal area 5 neuronal activity encodes movement kinematics, not movement dynamics. *Experimental Brain Research, 80,* 351–364.
Kalaska, J. F., & Crammond, D. J. (1992). Cerebral cortical mechanisms of reaching movements. *Science, 255,* 1517–1523.
Kalaska, J. F., & Hyde, M. L. (1985). Area 4 and area 5: Differences between the load direction-dependent discharge variability of cells during active postural fixation. *Experimental Brain Research, 59,* 197–202.
Kettner, R. E., Marcario, J., & Port, N. (1993). A neural network model of cortical activity during reaching. *Journal of Cognitive Neuroscience, 5,* 14–33.
Kettner, R. E., Schwartz, A. B., & Georgopoulos, A. P. (1988). Primate motor cortex and free arm movements to visual targets in three-dimensional space. III. Positional gradients and population coding of movement direction from various movement origins. *Journal of Neuroscience, 8,* 2938–2947.
Kuffler, S. W., & Hunt, C. C. (1952). The mammalian small-nerve fibers: A system for efferent nervous regulation of muscle spindle discharge. In P. Bard (Ed.), *Patterns of organization in the central nervous system* (pp. 24–47). Baltimore, MA. Williams & Wilkin.
Kuperstein, M. (1988). Neural model of adaptive hand-eye coordination for single postures. *Science, 239,* 1308–1311.
Lackner, J. R., & DiZio, P. (1994). Rapid adaptation to Coriolis force perturbations of arm trajectory. *Journal of Neurophysiology, 72,* 299–313.
Lackner, J. R., & Levine, M. S. (1978). Visual direction depends on the operation of spatial constancy mechanisms: The oculobrachial illusion. *Neuroscience Letters, 7,* 207–212.
Lackner, J. R., & Taublieb, A. B. (1984). Influence of vision on vibration-induced illusions of limb movement. *Experimental Neurology, 85,* 97–106.
Lacquaniti, F., Guigon, E., Bianchi, L., Ferraina, S., & Caminiti, R. (1995). Representing spatial information for limb movement: Role of area 5 in the monkey. *Cerebral Cortex, 5,* 391–409.
Loeb, G. E. (1985). Motoneurone task groups: Coping with kinematic heterogeneity. *Journal of Experimental Biology, 115,* 137–146.
Matthews, P. B. C. (1966). The reflex excitation of the soleus muscle of the decerebrate cat caused by vibration applied to its tendon. *Journal of Physiology, 184,* 450–472.
McCloskey, D. I. (1973). Differences between the senses of movement and position shown by the effects of loading and vibration of muscles in man. *Brain Research, 63,* 119–131.
McCloskey, D. I., Cross, M. J., Honner, R., & Potter, E. K. (1983). Sensory effects of pulling or vibrating exposed tendons in man. *Brain, 106,* 21–37.
Mel, B. W. (1991). A connectionist model may shed light on neural mechanisms for visually guided reaching. *Journal of Cognitive Neuroscience, 3,* 273–292.
Prochazka, A. (1992). A vital clue: Kinesthetic input is greatly enhanced in sensorimotor "vigilance." *Behavioral and Brain Sciences, 15,* 789–790.
Prochazka, A., Hulliger, M., Trend, P., & Dürmüller, N. (1988). Dynamic and static fusimotor set in various behavioral contexts. In P. Hník, T. Soukup, R. Vejsada, & J. Zelena (Eds.), *Mechanoreceptors: Development, structure, and function* (pp. 417–430). New York: Plenum.
Prochazka, A., Stephens, J. A., & Wand, P. (1979). Muscle spindle discharge in normal and obstructed movements. *Journal of Physiology, 287,* 57–66.
Roll, J. P., & Vedel, J. P. (1982). Kinaesthetic role of muscle afferents in man, studied by tendon vibration and microneurography. *Experimental Brain Research, 47,* 177–190.
Saltzman, E. L., & Kelso, J. A. S. (1987). Skilled actions: A task dynamic approach. *Psychological Review, 94,* 84–106.
Schwartz, A. B. (1992). Motor cortical activity during drawing movements: Single unit activity during sinusoid tracing. *Journal of Neurophysiology, 68,* 528–541.
Schwartz, A. B. (1993). Motor cortical activity during drawing movements: Population representation during sinusoid tracing. *Journal of Neurophysiology, 70,* 28–36.
Scott, S. H., & Kalaska, J. F. (1997). Reaching movements with similar hand paths but different arm orientations. I. Activity of individual cells in motor cortex. *Journal of Neurophysiology, 77,* 826–852.
Selverston, A. (1988). A consideration of invertebrate central pattern generators as computational databases. *Neural Networks, 2,* 109–117.
Sittig, A. C., Denier van der Gon, J. J., & Gielen, C. C. A. M. (1985). Separate control of arm position and velocity demonstrated by vibration of muscle tendon in man. *Experimental Brain Research, 60,* 445–453.
Smith, A. M. (1996). Does the cerebellum learn strategies for the optimal time-varying control of joint stiffness? *Behavioral and Brain Sciences, 19,* 399–410.
Woodworth, R. S. (1899). The accuracy of voluntary movement. *Psychological Review, 3,* 1–114.